Supplementary document - A fused canopy height map of Italy (2004–2024) from spaceborne and airborne LiDAR, and Landsat via deep learning and Bayesian averaging

Authors

Yang Su [1, 2, 3], Nikola Besic [4], Xianglin Zhang [3], Yidi Xu [2], Saverio Francini [5], Giovanni D'Amico [6], Gherardo Chirici [7, 8], Martin Schwartz [2], Ibrahim Fayad [2], Sarah Brood [1], Agnes Pellissier-tanon [2], Ke Yu [2], Haotian Chen [9, 3], Songchao Chen [10], Alexandre d'Aspremont [1], Philippe Ciais [2]

Affiliations

[1] CNRS & Département d'Informatique, École Normale Supérieure – PSL, 45 Rue d'Ulm, 75005 Paris, France

[2] Laboratoire des Sciences du Climat et de l'Environnement, CEA CNRS UVSQ Orme des Merisiers, 91190 Gif-sur-Yvette, France

[3] Université Paris-Saclay, AgroParisTech, INRAE, UMR ECOSYS, 91120 Palaiseau, France

[4] IGN, ENSG, Laboratoire d'inventaire forestier (LIF), 54000 Nancy, France

[5] Department of Science and Technology of Agriculture and Environment (DISTAL), University of Bologna, 40126 Bologna, Italy

[6] Department of Agriculture, Food, Environment and Forestry, Università degli Studi di Firenze, Via San Bonaventura, 13, 50145 Firenze, Italy

[7] Fondazione per il Futuro delle Città, Florence, Italy

[8] CNR Istituto dei Sistemi Complessi, Sesto Fiorentino (Florence), Italy

[9] Institute of Crop Sciences, Chinese Academy of Agricultural Sciences / Key Laboratory of Crop Physiology and Ecology, Ministry of Agriculture and Rural Affairs of China, Beijing 100081, China

[10] College of Environmental and Resource Sciences, Zhejiang University, 310058 Hangzhou, China

Corresponding Author

Yang Su yang.su@ens.fr +33 1 89 10 07 67 École Normale Supérieure – PSL

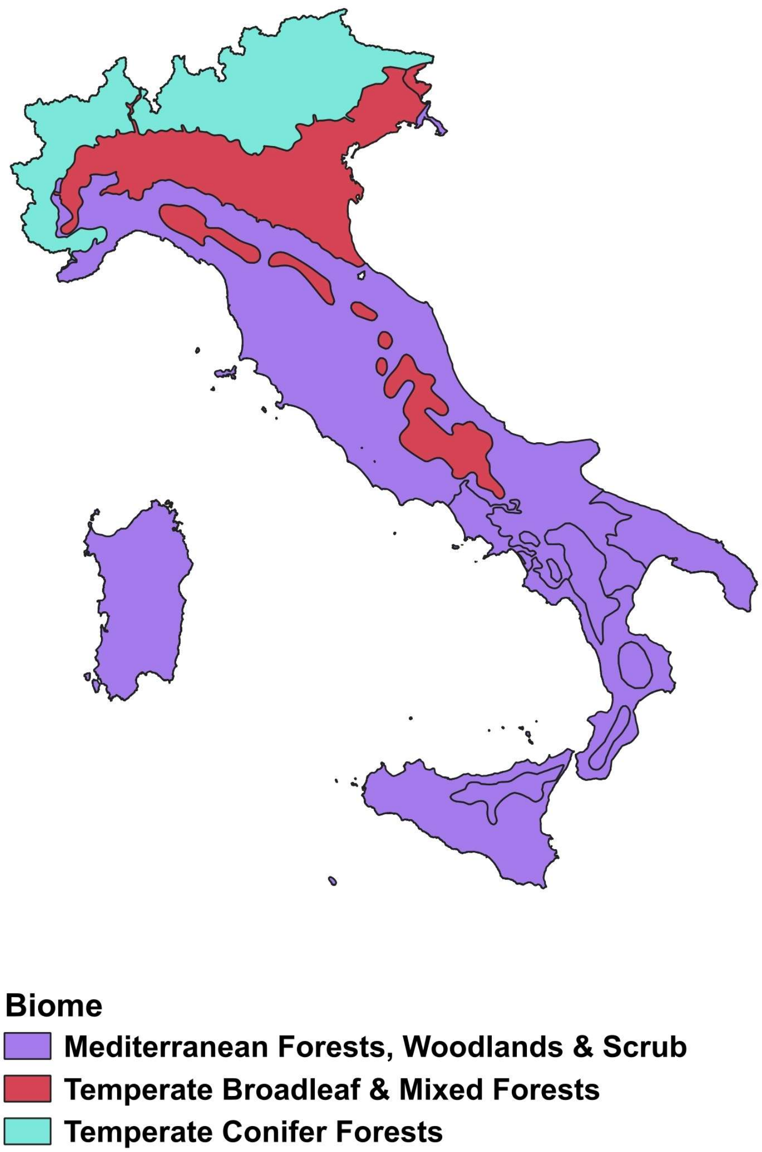

Figure S1 | Biomes across Italy.

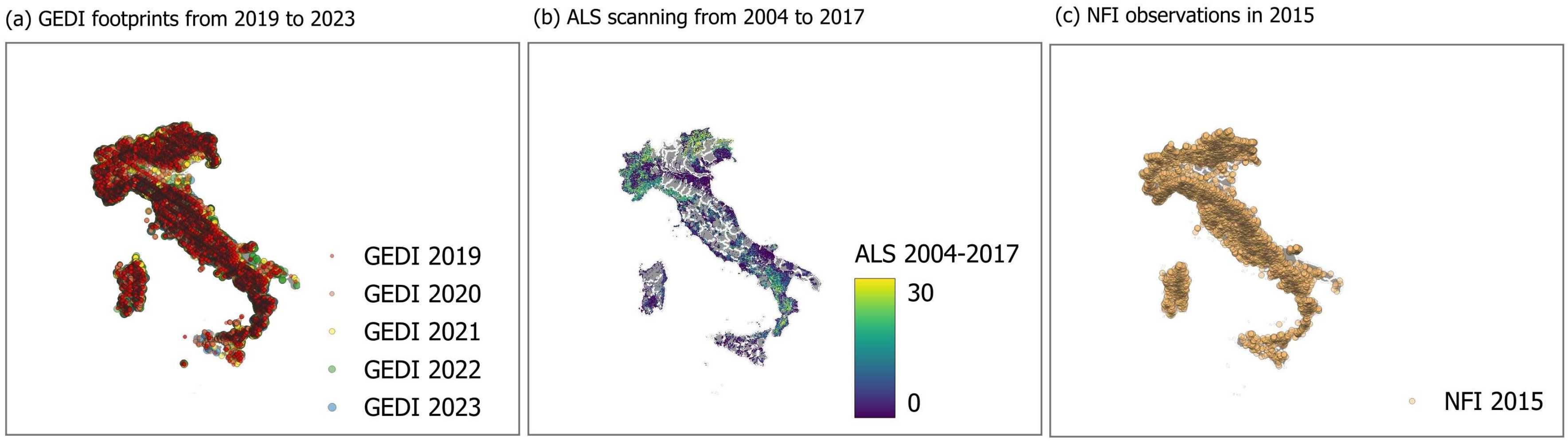

Figure S2 | Spatial coverage of GEDI, ALS and NFI datasets. Plot a is coverage of GEDI data from 2019 to 2023 (in total 1,485,449 footprints), plot b is the coverage of ALS data from 2004 to 2017 (16,858,373 ha), plot c is the coverage of NFI data fin 2015 (in total 6894 plots).

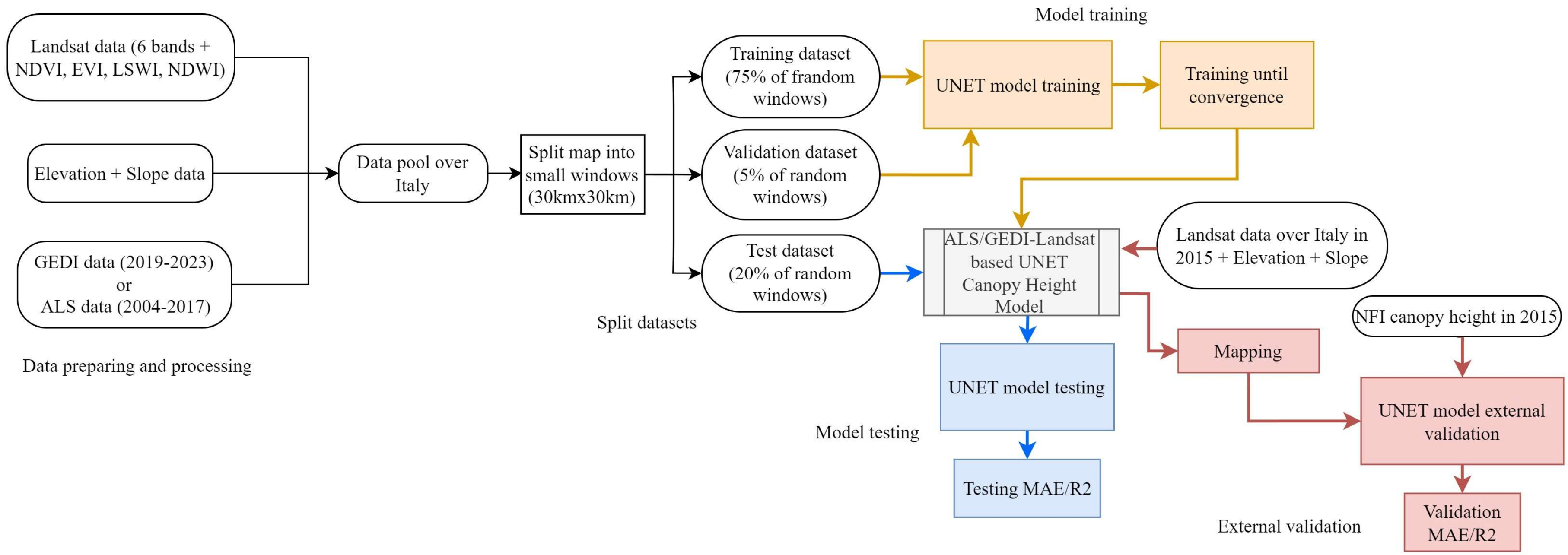

Figure S3 | Flow chart of training, testing and validation of UNET canopy height models. This plot showed the algorithm of UNET canopy height model training (marked by orange color), testing (marked by blue color) and external validation (marked by pink color) for ALS-Landsat based UNET model and the GEDI-Landsat based UNET model, respectively, depending on the input data.

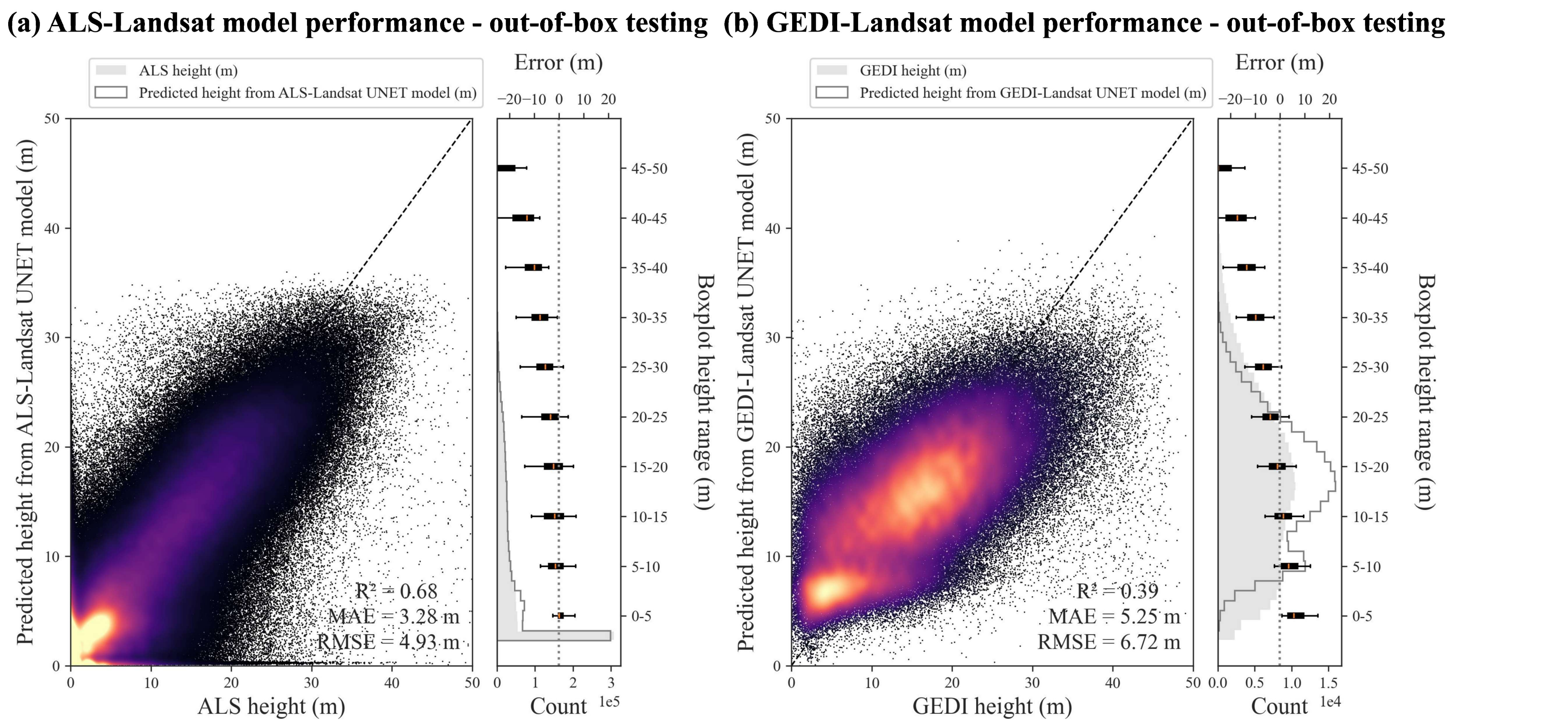

Figure S4 | Out-of-box testing of ALS-Landsat and GEDI-Landsat based UNET model. Plot a is scatterplot of predicted canopy heights of our ALS-Landsat based UNET canopy height model versus the canopy height of ALS data in the out-of-boxing testing dataset from 2004-2017. Plot b is scatterplot of predicted canopy heights of our GEDI-Landsat based UNET canopy height model versus the GEDI data in the out-of-boxing testing dataset from 2019-2023. The boxplots on the right side indicate the mean absolute errors in each height class.

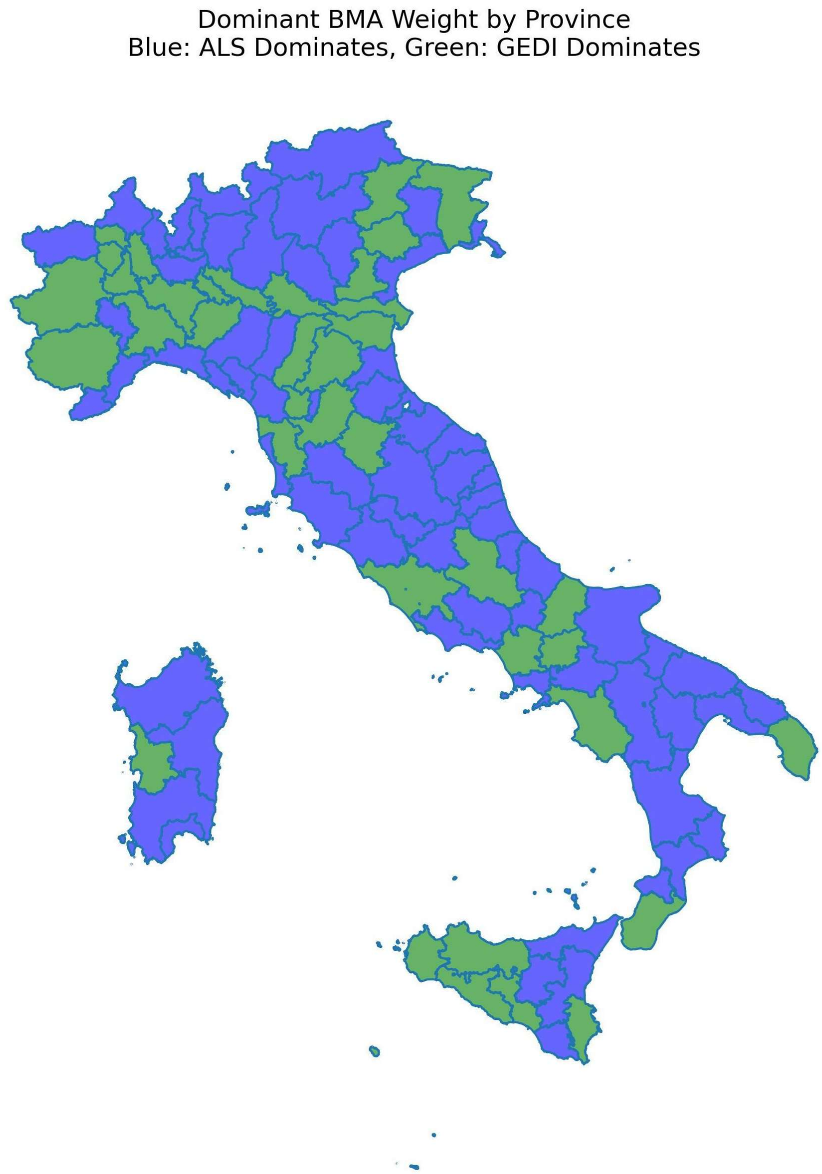

Figure S5 | The spatial distribution of dominant BMA weights across provinces. The blue area is the ALS dominated regions, while the green areas are the GEDI dominated regions.

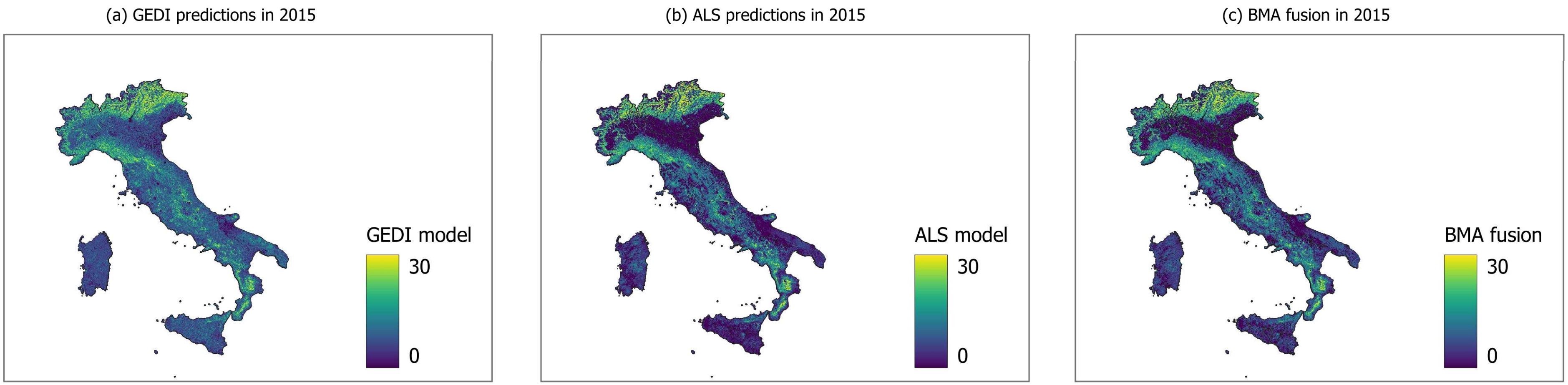

Figure S6 | Canopy height map of Italy at 30m resolution for the year 2015. Plot a is the nationwide spatial distribution of canopy height predicted with GEDI-Landsat based UNET model. Plot b is the nationwide spatial distribution of canopy height predicted with ALS-Landsat based UNET model. Plot c is the nationwide spatial distribution of canopy height produced with BMA fusion.

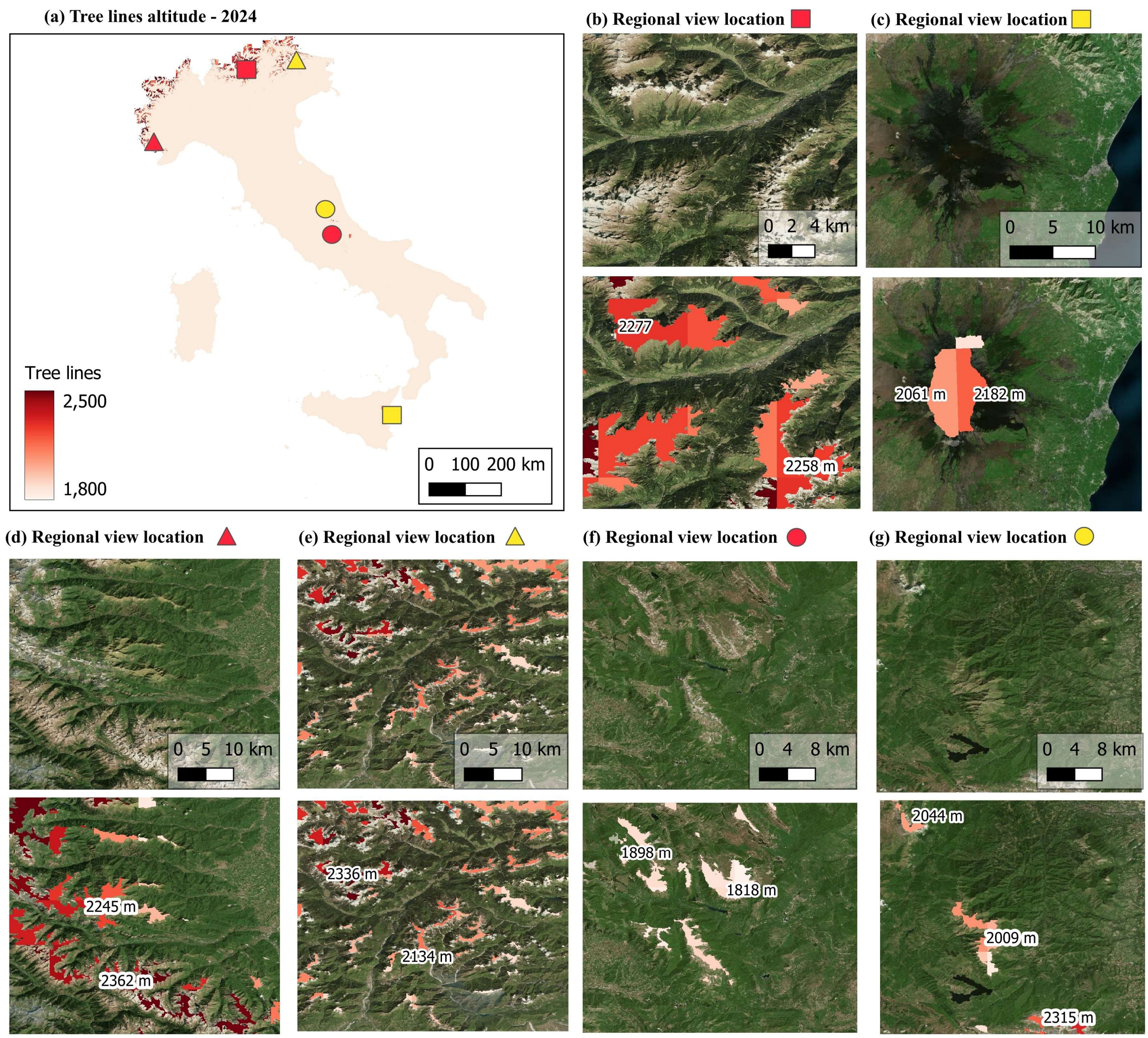

Figure S7 | Elevation of tree lines in 2024 over mountains. Plot a is the nationwide view of elevation of the tree lines over mountains. Plots b-g provide detailed comparisons between Landsat satellite imagery and detected tree lines across different environments.

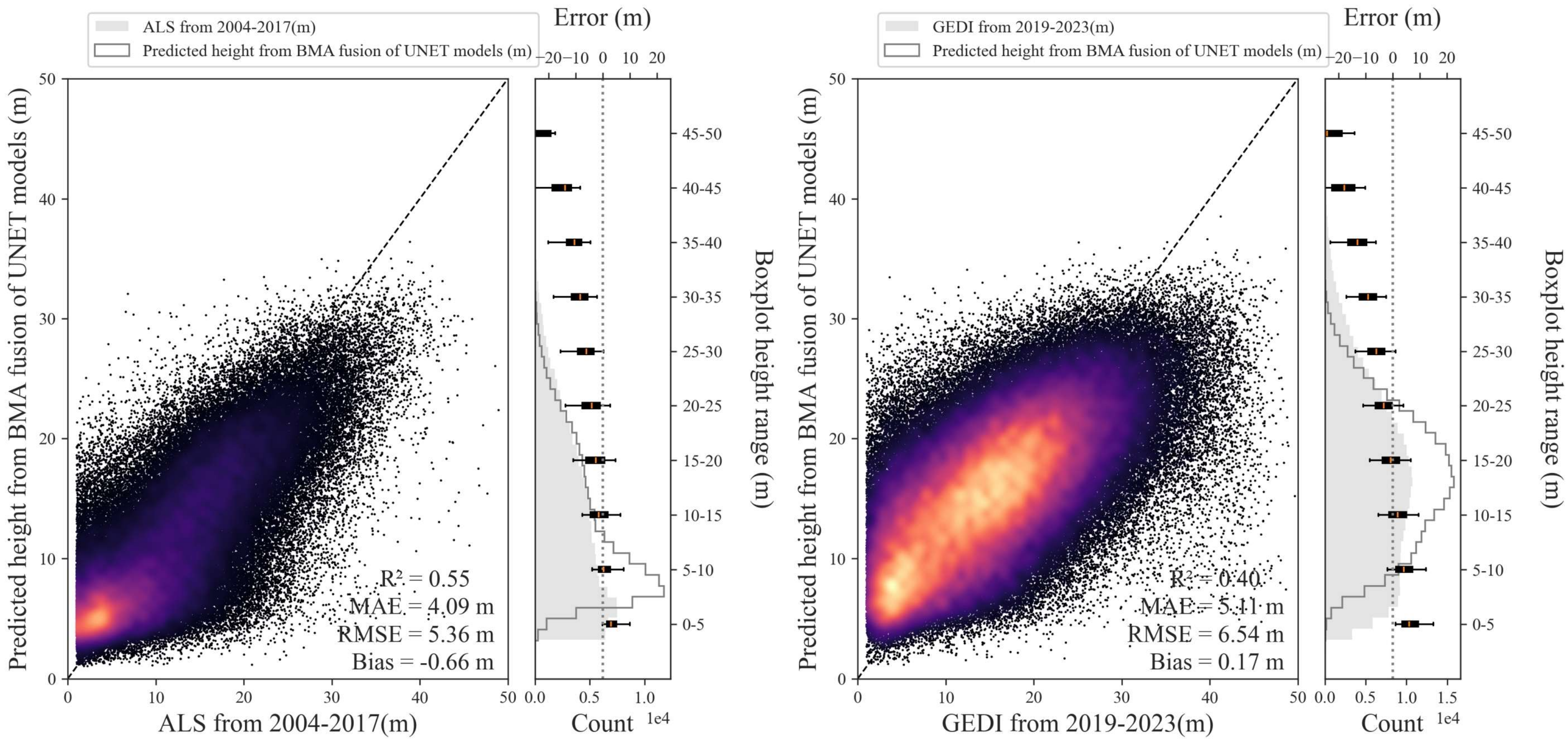

Figure S8 | Additional testing of BMA fusion products comparing with random sampled observations in ALS and GEDI dataset. Plot a is scatterplot of predicted canopy heights of BMA fused model versus the canopy height of ALS data from 2004-2017. Plot b is scatterplot of predicted canopy heights of BMA fused model versus the canopy height of ALS data from 2019-2023. The boxplots on the right side indicate the mean absolute errors in each height class. Note that each year, we sampled 10,000 observations in ALS and GEDI dataset.

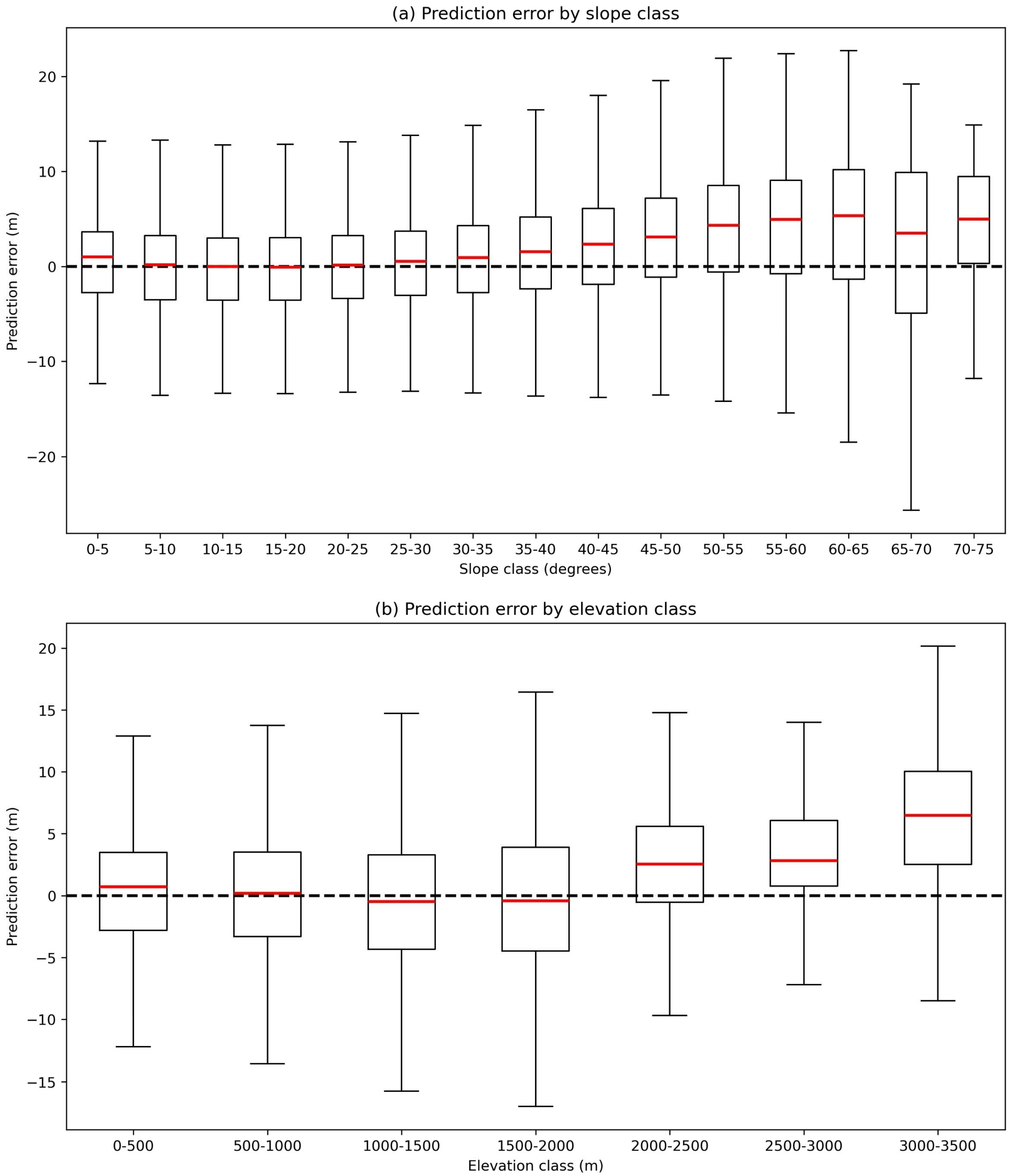

Figure S9 | Prediction errors of BMA products over different slope and elevation classes. Plot a is the prediction errors of BMA products over different slope classes when comparing with the random sampled ALS data in 2004-2017. Plot b is the prediction errors of BMA products over different elevation classes when comparing with the random sampled ALS data in 2004-2017. Note that each year, we sampled 10,000 observations in ALS dataset.

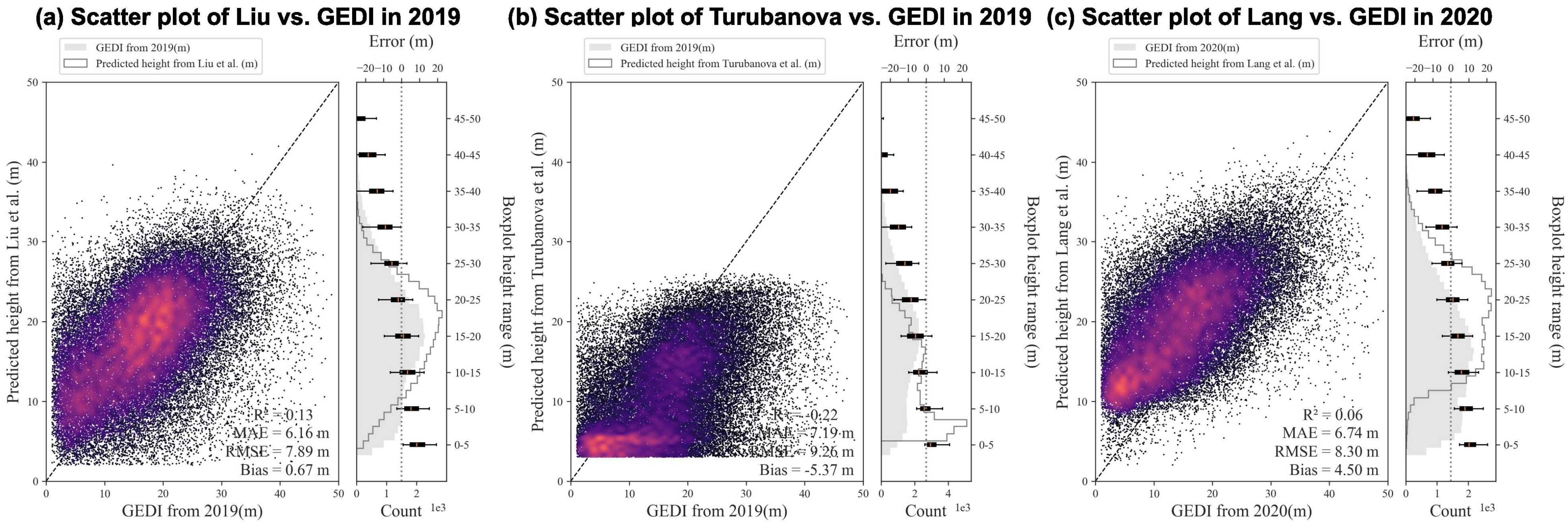

Figure S10 | Comparison between products of Liu et al. (Liu et al., 2023)**, Turubanova et al.** (Turubanova et al., 2023)**, and Lang et al.** (Lang et al., 2023) **with random sampled observations in GEDI dataset**. Plot a is scatterplot of predicted canopy heights of Liu et al. (Liu et al., 2023) versus the canopy height of GEDI data in 2019. Plot b is scatterplot of predicted canopy heights of Turubanova et al. (Turubanova et al., 2023) versus the canopy height of GEDI data in 2019. Plot c is scatterplot of predicted canopy heights of Lang et al. (Lang et al., 2023) versus the canopy height of GEDI data in 2020. The boxplots on the right side indicate the mean absolute errors in each height class. Note that each year, we sampled 10,000 observations in GEDI dataset.

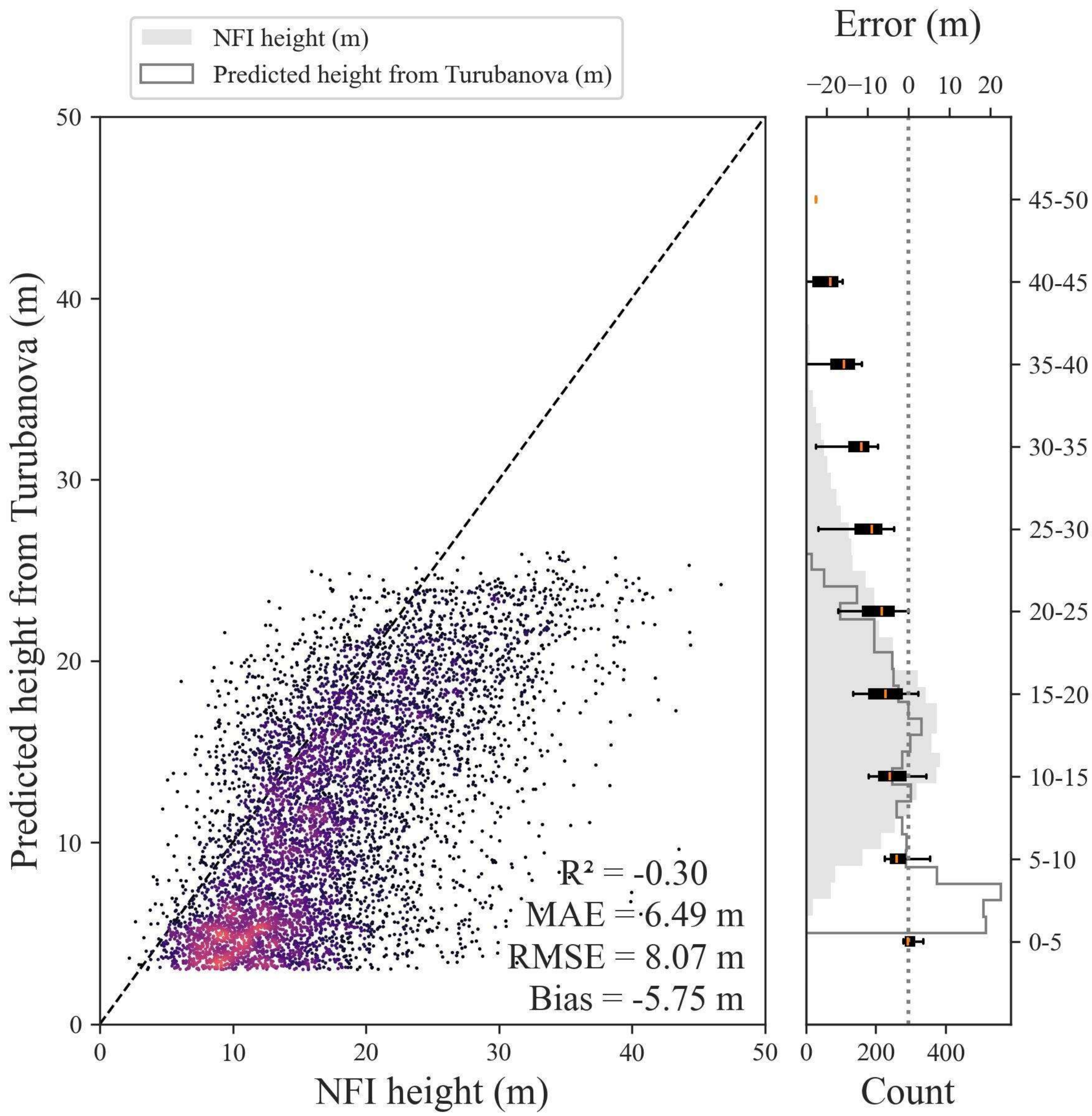

Figure S11 | External validation of the product from Turubanova et al. (Turubanova et al., 2023) **using NFI data in 2015**. This is scatterplot of predicted canopy heights of Turubanova et al. (Turubanova et al., 2023) in 2015 versus the canopy height of NFI observations in 2015 (Monitoring clearcutting and subsequent rapid recovery in Mediterranean coppice forests with Landsat time series. Zenodo repository. [dataset]., 2025; Chirici et al., 2020; Francini et al., 2021, 2022).

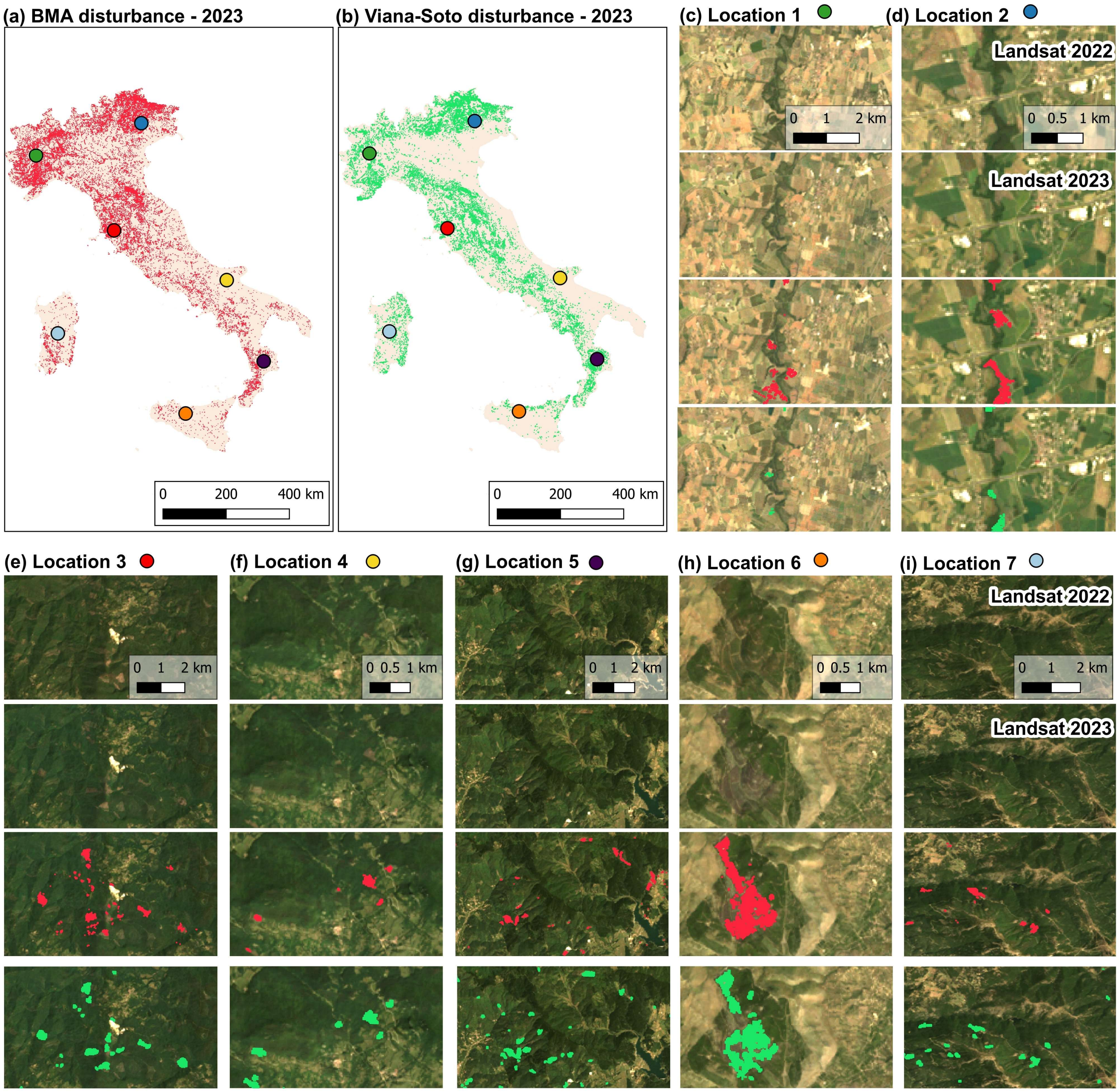

Figure S12 | Comparison of forest disturbance detection in 2022-2023 using the BMA product and Viana-Soto et al.'s dataset (Viana-Soto and Senf, 2024). Plot a is the annual forest disturbance map derived from interannual canopy height changes using the BMA product, plot b is the forest disturbance from Viana-Soto et al. (b). Plots c–i show detailed comparisons at selected locations across Italy (see colored markers in plots a and b). Each subpanel includes: Landsat imagery for 2022 (first row), Landsat imagery for 2023 (second row), and detected disturbance pixels from the BMA (red, third row) and Viana-Soto (green, forth row) datasets. These case studies demonstrate high consistency between the two products in detecting canopy loss across diverse landscapes, including agricultural mosaics, mountain forests, and intensively managed regions.

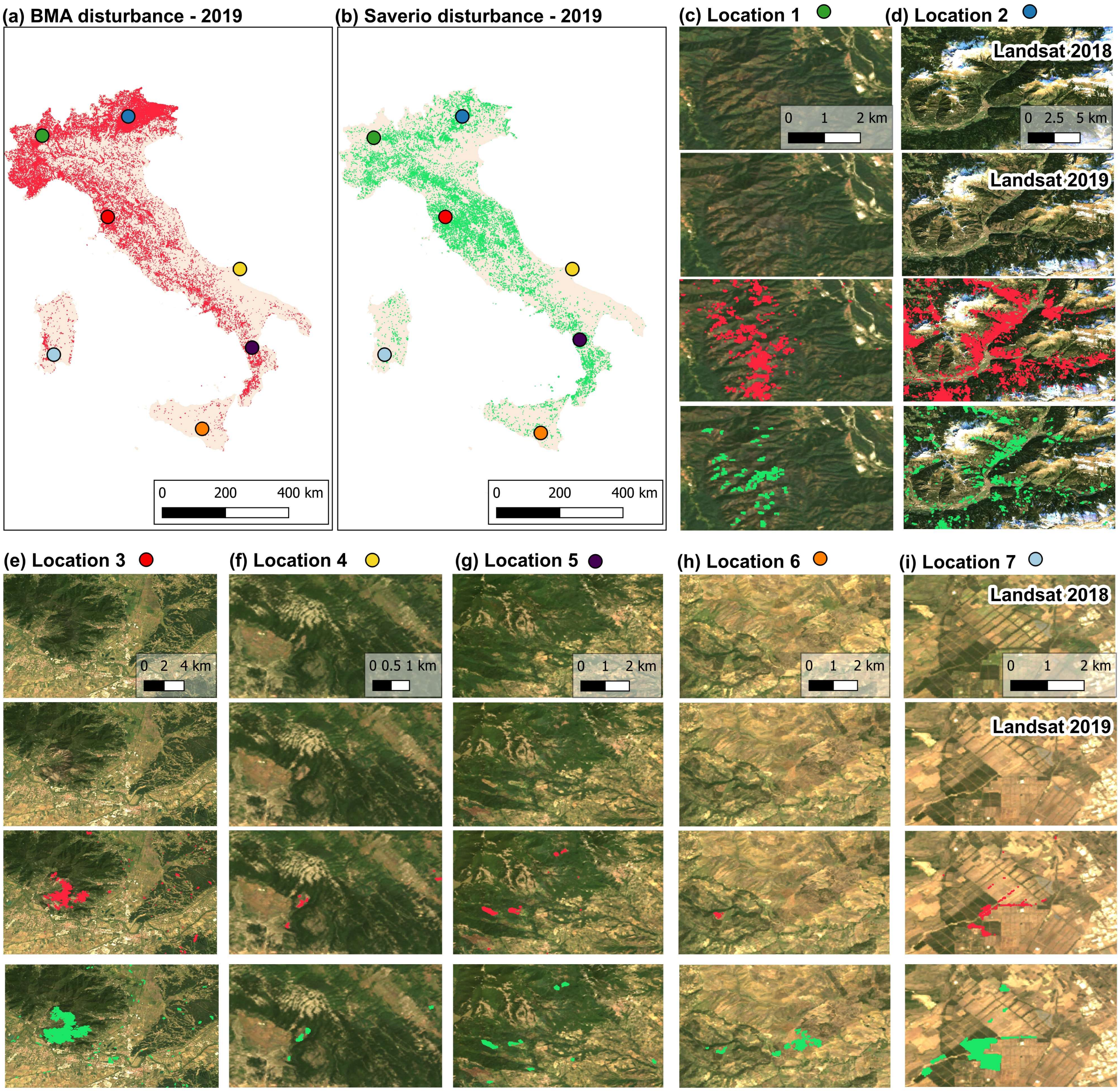

Figure S13 | Comparison of forest disturbance detection in 2018-2019 using the BMA product and Saverio et al.'s dataset (Francini and Chirici, 2022)**.** Plot a is the annual forest disturbance map derived from interannual canopy height changes using the BMA product, plot b is the forest disturbance from Saverio et al. (b). Plots c–i show detailed comparisons at selected locations across Italy (see colored markers in plots a and b). Each subpanel includes: Landsat imagery for 2018 (first row), Landsat imagery for 2019 (second row), and detected disturbance pixels from the BMA (red, third row) and Saverio (green, forth row) datasets. These case studies demonstrate high consistency between the two products in detecting canopy loss across diverse landscapes, including agricultural mosaics, mountain forests, and intensively managed regions.

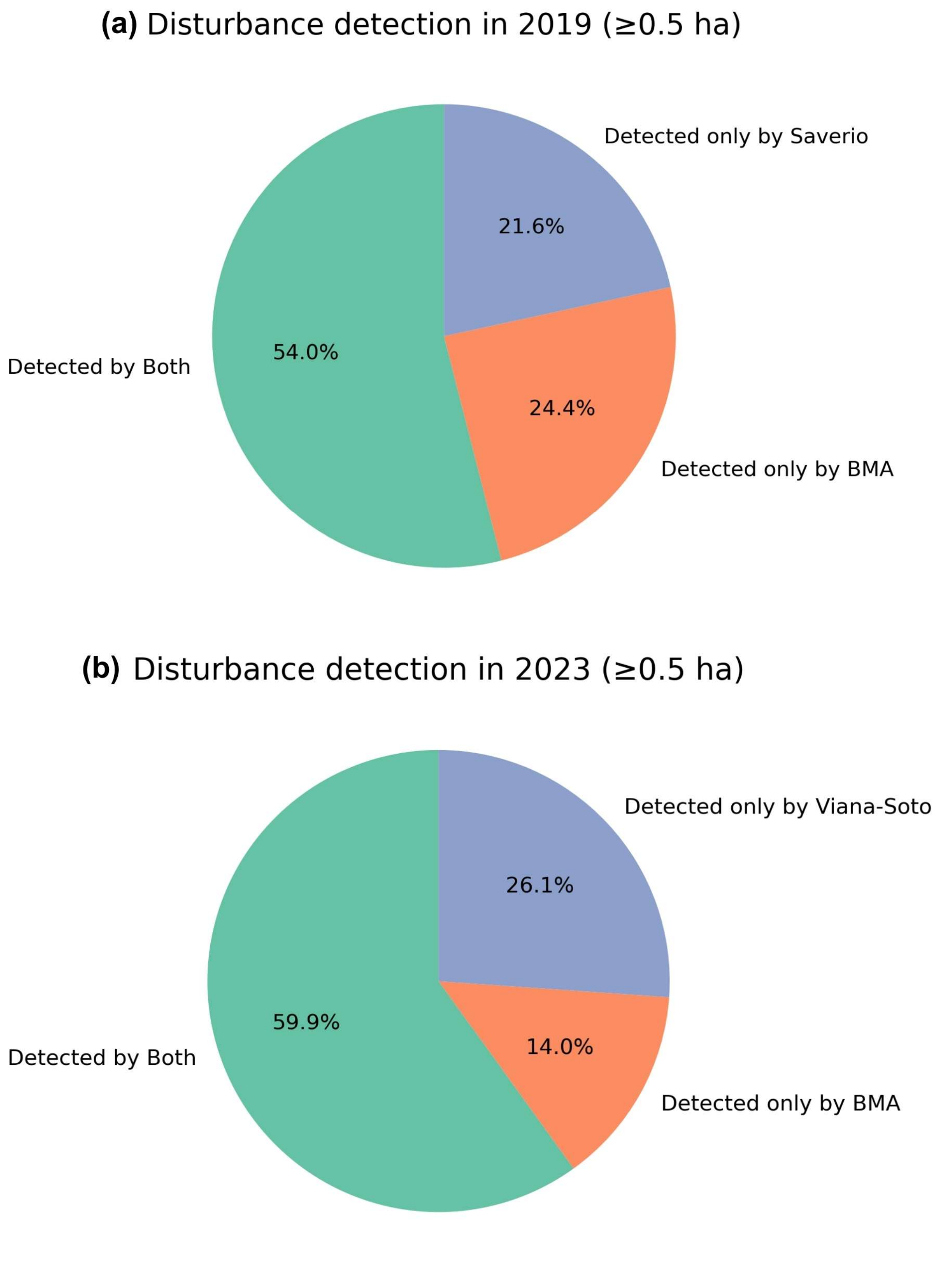

Figure S14 | Comparison of disturbance detection agreement between BMA-based and external products. Plot a is the Comparison for 2019 with the Sentinel-2-based disturbance map by Saverio et al. (Francini and Chirici, 2022), plot b is the Comparison for 2023 with the Landsat-based disturbance product by Viana-Soto et al. (Viana-Soto and Senf, 2024).

Supplementary tables

Table S1 | Main characteristics of ALS surveys available in Italy (D'Amico et al., 2021)

Id	**Data provider**	**Survey year**	**Survey area**	**Km²**	**Flight altitude**	**Density (pulse/m²)**	**Spatial resolution**	**Sensor**	**Sensor Wavelength (nm)**
1	Basilicata	2013	Basilicata	14382	900m	4	5x5	Riegl LMS Q680i	1550
2	Autonomous Province of Bolzano	2004 - 2006	South Tyrol	7411	850-1100m	0.6	2,5x2,5	TopoSys Falcon II and Optech Gemini ALTM 3033	1560 and 1064
3	Bosco Fontana	2006	Bosco Fontana	3	-	5.6	1x1 + point cloud	Optech ALTM 3100	1064
4	Municipality of Firenze	2017	Florence	102	915m	4	1x1	Riegl LMS-Q680i	1550
5	Autonomous Region of Fruli Venezia-Giulia	2006 - 2010	Fruli Venezia-Giulia	10420	180-3000m	4	1x1 + classified point cloud	Optech Gemini ALTM 3033	1064
6	LaMMA	2015	Tuscany forest windthrows 4-5/03/15	436	1100m	4.4	1x1 + classified point cloud	Riegl LMS-Q680i	1550

7	MATTM Contracts: 140, 145, 155, 172, 204, 208	2007 - 2016	National Rivers	24154339	-	-	1x1 + point cloud	ALTM Gemini, ALTM 3100, Pegasus	1064
8	MATTM Contracts: 140, 176	2008 - 2012	Coast line	1926671	-	-	2x2 + point cloud	ALTM Gemini, ALTM 3100, Pegasus	1064
9	Piemonte	2009 - 2011	Piemonte	2.92E+08	4500m	0.5	5x5 + point cloud	LEICA ALS50-II (Leica Geosystems 2006)	1064
10	Autonomous Region of Sardegna	2008	Alghero	666	800m	1	5x5	Riegl LMS-Q560	NIR
11	Autonomous Region of Sardegna	2008	Coast	5579	1400m	1	1x1	Optech Gemini ALTM	1064
12	Autonomous Region of Sardegna	2009	Ogliastra	318	800m	5	1x1 + point cloud	Riegl LMS-Q560	NIR
13	Autonomous Region of Sardegna	2013	Urban centers	15415	700m	4	1x1	Riegl LMS Q680i	1550

14	Toscana, Province of Arezzo	2004	Arno, Tevere.	89	1200m	0.5-1.5	2x2	Optech Gemini ALTM 3033	1064
15	Toscana Serchio basin authority	2005	Canale Ozzeri, Rio Guappero	31	1200m	1	1x1	Optech Gemini ALTM 3032	1064
16	Toscana Serchio basin authority	2006	Serchio and main tributaries	12435	1200m	1	1x1	Optech Gemini ALTM 3033	1064
17	Toscana	2006-2007	Mugello, Sieve	305	1200m	1	1x1	Optech Gemini ALTM 3033	1064
18	Toscana, Province of Siena	2007	Ombrone, Arbia	35	1500m	1	1x1	Optech Gemini	1064
19	Toscana, Arno basin authority	2008	Elsa, Ombrone, Bisenzio, Sieve	913	1200m	1.5	1x1	ALTM Gemini	1064
20	Toscana, Arno basin authority	2008	Monti della Calvana	314	2300m	0.4	3x3	ALTM Gemini	1064
21	Toscana, Arno basin authority	2009	Monti della Calvana	314	2300m	0.4	2x2	ALTM Gemini	1064

22	Toscana	2010	Lunigiana, Pistoia, Lucca, Scarlino	1923	-	0.5	1x1	Optech Gemini ALTM and Optech Pegasus ALTM	1064 and 1064
23	Toscana	2011	Aulla	85	1800-1900m	0.5	1x1	Optech Gemini	1064
24	Toscana	2012	Carrara, Pienza, Minucciano, Vagli	101	1600m	1.7	1x1	Optech Gemini ALTM and Optech Pegasus ALTM	1064 and 1064
25	Toscana	2012	Magra	54	1400m	1.5	1x1	Optech Pegasus	1064
26	Toscana	2012	Teglia, Osca, Mangiola	26	1050m	1.5	1x1	Optech Gemini	1064
27	Autonomous Province of Trento	2006	Trentino excluded Adige river	6702	1000-1800m	1.8	1x1 + point cloud	Optech ALTM 3100	1064
28	Autonomous Province of Trento	2009	Adige river	636	1500m	0.5	1x1 + point cloud	TopoSys Falcon II	1560
29	Autonomous Region of Valle d'Aosta	2008	Valle d'Aosta	3620	2700-4700m	2	2x2 + point cloud	Optech Gemini ALTM	1064

Table S1 | UNET model architecture in our study – Encoder, Bottleneck, Decoder

Step	Layer	Input Size	Output Size	Kernel/Operation	Channels
1	inc (DoubleConv)	H × W × n_channels	H × W × 64	3×3 Conv, ReLU (twice)	64
2	down1 (Down)	H × W × 64	H/2 × W/2 × 128	2×2 Max Pool + 3×3 Conv, ReLU (twice)	128
3	down2 (Down)	H/2 × W/2 × 128	H/4 × W/4 × 256	2×2 Max Pool + 3×3 Conv, ReLU (twice)	256
4	down3 (Down)	H/4 × W/4 × 256	H/8 × W/8 × 512	2×2 Max Pool + 3×3 Conv, ReLU (twice)	512
5	down4 (Down)	H/8 × W/8 × 512	H/16 × W/16 × 1024 (or 512 if bilinear)	2×2 Max Pool + 3×3 Conv, ReLU (twice)	512
6	down4 (Bottleneck)	H/16 × W/16 × 512	H/16 × W/16 × 512	3×3 Conv, ReLU (twice)	512
7	up1 (Up)	H/16 × W/16 × 512	H/8 × W/8 ×256	2×2 Up-conv, Skip Connection, 3×3 Conv, ReLU (twice)	256
8	up2 (Up)	H/8 × W/8 × 256	H/4 × W/4 × 128	2×2 Up-conv, Skip Connection, 3×3 Conv, ReLU (twice)	128
9	up3 (Up)	H/4 × W/4 × 128	H/2 × W/2 × 64	2×2 Up-conv, Skip Connection, 3×3 Conv, ReLU (twice)	64
10	up4 (Up)	H/2 × W/2 × 64	H × W × 64	2×2 Up-conv, Skip Connection, 3×3 Conv, ReLU (twice)	64

Table S2 | UNET model settings

Parameter	Value
Optimizer	Adam
Initial Learning Rate	0.01
Learning Rate Decay	Reduce by 0.9 every 10 loops if no improvement
Loss Function	Mean Absolute Error (MAE)

References

Monitoring clearcutting and subsequent rapid recovery in Mediterranean coppice forests with Landsat time series. Zenodo repository. [dataset]. https://doi.org/10.5281/zenodo.3689194, 2020.

Chirici, G., Giannetti, F., Mazza, E., Francini, S., Travaglini, D., Pegna, R., and White, J. C.: Monitoring clearcutting and subsequent rapid recovery in Mediterranean coppice forests with Landsat time series, Ann For Sci, 77, 40, https://doi.org/10.1007/s13595-020-00936-2, 2020.

D'Amico, G., Vangi, E., Francini, S., Giannetti, F., Nicolaci, A., Travaglini, D., Massai, L., Giambastiani, Y., Terranova, C., and Chirici, G.: Are we ready for a National Forest Information System? State of the art of forest maps and airborne laser scanning data availability in Italy, IForest, 14, 144–154, https://doi.org/10.3832/ifor3648-014, 2021.

Francini, S. and Chirici, G.: A Sentinel-2 derived dataset of forest disturbances occurred in Italy between 2017 and 2020, Data Brief, 42, 108297, https://doi.org/10.1016/j.dib.2022.108297, 2022.

Francini, S., McRoberts, R. E., Giannetti, F., Marchetti, M., Scarascia Mugnozza, G., and Chirici, G.: The Three Indices Three Dimensions (3I3D) algorithm: a new method for forest disturbance mapping and area estimation based on optical remotely sensed imagery, Int J Remote Sens, 42, 4693–4711, https://doi.org/10.1080/01431161.2021.1899334, 2021.

Francini, S., D'Amico, G., Vangi, E., Borghi, C., and Chirici, G.: Integrating GEDI and Landsat: Spaceborne Lidar and Four Decades of Optical Imagery for the Analysis of Forest Disturbances and Biomass Changes in Italy, Sensors, 22, 2015, https://doi.org/10.3390/s22052015, 2022.

Lang, N., Jetz, W., Schindler, K., and Wegner, J. D.: A high-resolution canopy height model of the Earth, Nat Ecol Evol, 7, 1778–1789, https://doi.org/10.1038/s41559-023-02206-6, 2023.

Liu, S., Brandt, M., Nord-Larsen, T., Chave, J., Reiner, F., Lang, N., Tong, X., Ciais, P., Igel, C., Pascual, A., Guerra-Hernandez, J., Li, S., Mugabowindekwe, M., Saatchi, S., Yue, Y., Chen, Z., and Fensholt, R.: The overlooked contribution of trees outside forests to tree cover and woody biomass across Europe, Sci Adv, 9, https://doi.org/10.1126/sciadv.adh4097, 2023.

Turubanova, S., Potapov, P., Hansen, M. C., Li, X., Tyukavina, A., Pickens, A. H., Hernandez-Serna, A., Arranz, A. P., Guerra-Hernandez, J., Senf, C., Häme, T., Valbuena, R., Eklundh, L., Brovkina, O., Navrátilová, B., Novotný, J., Harris, N., and Stolle, F.: Tree canopy extent and height change in Europe, 2001–2021, quantified using Landsat data archive, Remote Sens Environ, 298, 113797, https://doi.org/10.1016/j.rse.2023.113797, 2023.

Viana-Soto, A. and Senf, C.: The European Forest Disturbance Atlas: a forest disturbance monitoring system using the Landsat archive, https://doi.org/10.5194/essd-2024-361, 21 November 2024.